Biophysical Journal
Article

Biophysical Society

Binding by TRBP-dsRBD2 Does Not Induce Bending of Double-Stranded RNA

Roderico Acevedo,[1,2] Declan Evans,[1,2] Katheryn A. Penrod,[1,2] and Scott A. Showalter[1,2,3,*]
[1]Department of Chemistry, [2]Center for RNA Molecular Biology, and [3]Department of Biochemistry and Molecular Biology, The Pennsylvania State University, University Park, Pennsylvania

ABSTRACT Protein-nucleic acid interactions are central to a variety of biological processes, many of which involve large-scale conformational changes that lead to bending of the nucleic acid helix. Here, we focus on the nonsequence-specific protein TRBP, whose double-stranded RNA-binding domains (dsRBDs) interact with the A-form geometry of double-stranded RNA (dsRNA). Crystal structures of dsRBD-dsRNA interactions suggest that the dsRNA helix must bend in such a way that its major groove expands to conform to the dsRBD's binding surface. We show through isothermal titration calorimetry experiments that dsRBD2 of TRBP binds dsRNA with a temperature-independent observed binding affinity (K_D ~500 nM). Furthermore, a near-zero observed heat capacity change ($\Delta C_p = 70 \pm 40$ cal·mol^{-1}·K^{-1}) suggests that large-scale conformational changes do not occur upon binding. This result is bolstered by molecular-dynamics simulations in which dsRBD-dsRNA interactions generate only modest bending of the RNA along its helical axis. Overall, these results suggest that this particular dsRBD-dsRNA interaction produces little to no change in the A-form geometry of dsRNA in solution. These results further support our previous hypothesis, based on extensive gel-shift assays, that TRBP preferentially binds to sites of nearly ideal A-form structure while being excluded from sites of local deformation in the RNA helical structure. The implications of this mechanism for efficient micro-RNA processing will be discussed.

INTRODUCTION

Double-stranded RNA-binding domains (dsRBDs) play an important role in gene regulation, polyadenylation of messenger RNA, signal recognition, nuclear targeting, and, most significantly for this study, RNA processing (1,2). Specifically, there are 10 dsRBDs associated with the canonical micro-RNA (miRNA) maturation pathway, and at least one of these is found in each of the five proteins that are central to the pathway. In general, mature miRNA is formed from long-hairpin RNAs (~44 bp in length) that are processed by two cleavage events into single-stranded RNAs (~21 nt in length). Once generated, the mature miRNA is guided by the RNA-induced silencing complex to bind with high sequence specificity to mRNA and to regulate protein expression (3). Given the biological implications of misregulation of the sequence specificity of miRNA interactions, which is certain to arise if cuts are inaccurately placed, it is intriguing that the molecular machinery of miRNA processing makes abundant use of the dsRBD motif. In general, dsRBDs are known to recognize double-stranded RNA (dsRNA) by shape, and dsRBDs seldom display sequence specificity, although exceptions do exist (4). Significantly, our laboratory (5–7) and others (8–11) have extensively investigated multiple dsRBDs from the miRNA processing pathway and confirmed that when they are capable of binding dsRNA, the dsRBD motifs from these proteins follow the general trend of binding through structural recognition of the A-form geometry. Although this type of recognition does allow dsRBDs to interact with diverse sets of substrates, it is not obvious how their use facilitates enhanced cleavage efficiency and fidelity, as has been demonstrated for pre-miRNA processing by the RNase III enzyme Dicer in the presence of its cofactor protein TRBP (12,13). Motivated by the need to understand in detail how TRBP contributes to substrate dsRNA shape recognition, we investigated in vitro interactions of TRBP with a wide variety of substrates, some of which contained only Watson-Crick basepairs and others of which contained asymmetric bulges and noncanonical basepairs (7). In summary, our previous work demonstrated that when the two N-terminal dsRBDs of TRBP bind to RNA, they are excluded from bulges and internal loops, which has the effect of positioning TRBP on the dsRNA substrates that it will present to Dicer.

Submitted March 10, 2016, and accepted for publication May 9, 2016.
*Correspondence: sas76@psu.edu
Editor: James Cole.
http://dx.doi.org/10.1016/j.bpj.2016.05.012

Our finding that TRBP binds preferentially to Watson-Crick duplexes that should possess a relatively ideal A-form geometry is at odds with trends observed in multiple crystal structures of dsRBD-dsRNA complexes, including that of TRBP-dsRBD2 itself, in which two 10-mer dsRNA duplexes align to form a structure reminiscent of a continuous dsRNA. These cocrystal structures led to the hypothesis that dsRBDs induce strong bends into the A-form geometry of the dsRNA they bind. The earliest structure of this type was that of the second dsRBD of *Xenopus laevis* RNA binding protein A (Xlrbpa-2) bound to a GC 10-mer dsRNA (Fig. 1 *A*) (14). Xlrbpa-2 displays the canonical dsRBD fold (α_1-β_1-β_2-β_3-α_2) and contacts the RNA in three regions: the residues in helix 1 interact with the 2′ hydroxyls along minor groove I, those in loop 2 contact the 2′ hydroxyls along minor groove II, and residues in helix 2 contact the backbone phosphates projecting into the major groove. Close investigation of the structure reveals that an observed 3 Å deformation of the major-groove width is caused by a staggering of the two helices by ~5 Å to permit the deviation. Ryter and Schultz (14) noted that for Xlrbpa-2 dsRBD, this widened major groove is necessary to accommodate a protein-RNA interaction. In analogy to the Xlrbpa-2 result, the crystal structure of TRBP-dsRBD2 bound to a GC 10-mer dsRNA also reveals TRBP-dsRBD2 bridging two coaxially stacked dsRNA helices, with helix 2 bridging a larger-than-usual major groove (Fig. 1 *B*) (15). These two crystal structures seem to validate the hypothesis that dsRBD-dsRNA interactions are accompanied by conformational changes in the RNA helix geometry. In contrast, the structures of *Aquifex aeolicus* RNase III and the two dsRBDs from ADAR2 bound to RNA do not feature any distortion of the A-form geometry (16,17), calling into question the generality of the bending model and the applicability of distortions observed when 10-mer duplexes coaxially stack. Given that the introduction of distorted dsRNA geometry by TRBP binding may impact the efficiency and/or specificity of cleavage by Dicer, we aimed to test whether TRBP-dsRBD2 introduces a bend into dsRNA upon binding in solution.

If major-groove deformations are imposed by TRBP binding in solution, then spectroscopic and calorimetric signatures of their formation should be measurable by standard biophysical techniques. For example, circular dichroism (CD) spectroscopy is a technique that is commonly used to assess the secondary-structural features of chiral biomolecules (18), and was used to validate the bending hypothesis derived from the Xlrbpa2-dsRNA crystal structure (14). For protein-nucleic acid interactions in general, an experimental paradigm has been established whereby changes in the nucleic acid ellipticity serve as the source of signal, because ellipticity is inversely proportional to the winding angle of the helix (19). This mechanism has been leveraged as a source of signal in experiments that aimed to determine the saturating stoichiometry of the dsRBD-dsRNA interaction, yielding stoichiometries in good agreement with those determined by orthogonal techniques such as analytical ultracentrifugation (19). Indeed, in a previous study employing a similar CD experiment (7), we also reported the stoichiometry of TRBP binding to dsRNAs of various lengths (Fig. 1 *C*). Interestingly, we observed a change in CD signal upon TRBP binding, which suggests that although TRBP may be excluded from sites of substantial molecular deviation from A-form geometry, the protein is nonetheless able to

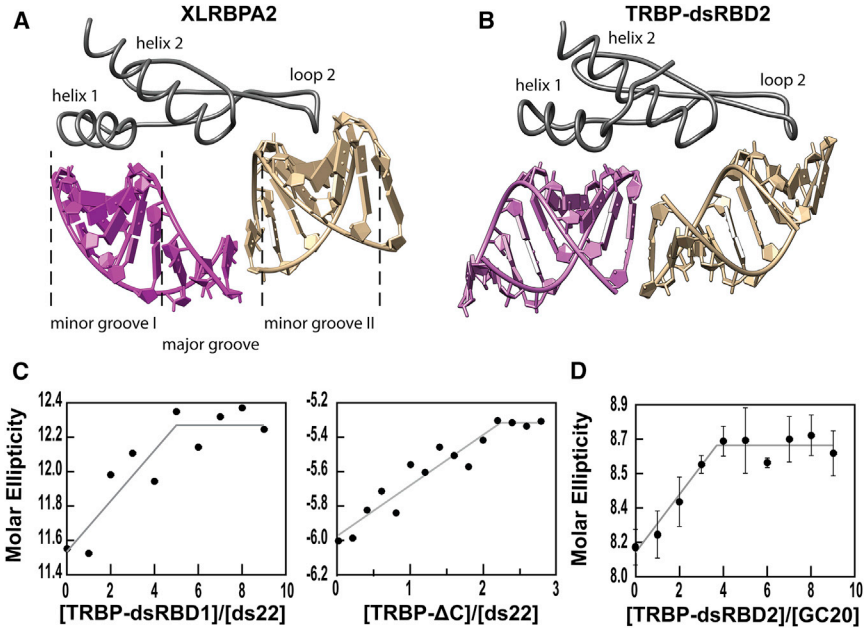

FIGURE 1 Crystal structures of dsRBD-dsRNA complexes promote the hypothesis that dsRBD-binding bends dsRNA. (*A*) Crystal structure of dsRBD2 of Xlrbpa from *Xenopus laevis* bound to GC10-mer RNA (PDB: 1DI2) and (*B*) the crystal structure of dsRBD2 of TRBP bound to GC 10-mer RNA (PDB: 3ADL). Both proteins (*grey, ribbons*) display the αββββα fold of a dsRBD. Helix 1, loop 2, and helix 2 are labeled for ease of reference when discussed in the text. It is noteworthy that helix 2 bridges the span between two co-axially stacked helices. (*C*) Stiochiometric titration of TRBP-dsRBD1 (*left*) and TRBP-ΔC (*right*) into 22-mer RNA from previous work (7). (*D*) Stiochiometric titration of TRBP-dsRBD2 into GC20 RNA solution. Data points are the average of three independent experiments with error bars depicting two standard deviations from the mean. Break point analyses for all titrations were performed in MATLAB as described in the Materials and Methods. To see this figure in color, go online.

accommodate, or even induce, some amount of structural deformation in substrate dsRNA.

In this study, we aimed to resolve the outstanding question of whether the mechanism of dsRNA binding by TRBP includes the introduction of a bend into the dsRNA. This objective was met through the use of isothermal titration calorimetry (ITC) supplemented by molecular-dynamics (MD) simulations. We conducted our studies using TRBP-dsRBD2 and a 20-mer duplex RNA we named GC20, which was designed to mimic the pair of 10-mers minimal substrate implied by the Xlrbpa-2 and TRBP-dsRBD2 cocrystal structures. The temperature-dependent ITC experiments we present reveal that binding occurs in a temperature-independent manner, as reflected by the invariant apparent equilibrium dissociation constant (K_D) and near-zero observed specific heat of binding (ΔC_p), which suggest that large-scale conformational changes are not associated with the binding event. These results are supported by the MD simulations, which indicate that protein association does not lead to large-scale conformational changes in the dsRNA. Specifically, there are no appreciable groove-width differences between the apo-RNA and holo-RNA trajectories. Taken together, these results suggest that the TRBP-dsRNA interaction produces little to no change in the overall geometry of the RNA helix.

MATERIALS AND METHODS

Sample preparation

TRBP-dsRBD2 (residues 159–235 of the human protein) was expressed and purified as previously described (7). A self-complementary synthetic RNA, GC20, was ordered from Dharmacon (GE Healthcare, Chicago, IL), with sequence 5′-GCGCGCGCGCGCGCGCGCGC-3′. Deprotection of the RNA was performed according to the protocol provided by the manufacturer. The concentration and purity of the RNA were determined by UV spectroscopy using an extinction coefficient of 165,000 $L \cdot mol^{-1} \cdot cm^{-1}$. Subsequently, the RNA was duplexed by heat denaturation at 90°C for 45 s, followed by fast annealing at 4°C for 5 min.

CD spectroscopy

CD experiments were performed on a Jasco (Easton, MD) J-810 spectrophotometer with a 2 mm path-length quartz cuvette using a previously established measurement protocol (7) and the fitting procedure of Ucci et al. (19). Experiments were done in triplicate and the data points are presented here with error bars representing two standard deviations from the mean.

Differential scanning calorimetry

To determine an appropriate range of temperatures for the subsequent ITC experiments, we monitored the thermal stabilities of TRBP-dsRBD2 and GC20 by differential scanning calorimetry (DSC) using a MicroCal VP-Capillary DSC (Malvern, Westborough, MA). Each species was extensively dialyzed in ITC buffer (50 mM sodium cacodylate pH 7.0, 50 mM potassium glutamate), yielding samples with final concentrations of 80 μM TRBP-dsRBD2 and 45 μM GC20. In each experiment, the biomolecular solution was heated from 30°C to 80°C and monitored with a scan rate of 90°C per hour. A reference experiment using only ITC buffer was run for buffer subtraction before peak determination using the cursor-initiated non-two-state program in the Origin 7.0 DSC software. After fitting was done in Origin, the resulting data sets were plotted using in-house-written MATLAB (The MathWorks, Natick, MA) scripts. Experiments were done in triplicate before averaging; for the best-fit parameters and their associated uncertainties, see Table S1 in the Supporting Material.

ITC

Calorimetry experiments were conducted on a MicroCal VP-ITC calorimeter (Malvern). Protein constructs and duplexed RNA were codialyzed in ITC buffer (50 mM sodium cacodylate pH 7.0, 50 mM potassium glutamate) overnight. TRBP-dsRBD2 was diluted to working conditions (see Table 1) and added to the syringe. The GC20 dsRNA was diluted to a 1 μM duplex concentration and then placed in the sample cell. Experiments were performed at 10°C, 15°C, 20°C, and 25°C (which was chosen as the upper limit based on the temperature at which the thermal denaturation of TRBP-dsRBD2 began to emerge in the DSC traces). All experiments were analyzed using the one-set-of-sites model in MATLAB as previously described (20). The resulting best-fit parameters yielded the equilibrium association constant (K_A, reported here as its inverse: $K_D = K_A^{-1}$), the overall change in the enthalpy of the system (ΔH), and the apparent binding stoichiometry (n). These parameters were used to derive the Gibbs free energy of binding using the relationship $\Delta G = RT \cdot \ln(K_D)$, and the overall change in the entropy of the system, using the experimental temperature and the relationship $\Delta G = \Delta H - T\Delta S$. All titrations were performed in triplicate for each experimental temperature, and the average of each resulting best-fit parameter computed. The averages are reported here with their associated errors (calculated by standard error propagation methods).

Atomistic simulations for MD

Two systems were built to investigate dsRNA bending upon interaction with TRBP: 1) the GC 20-mer of dsRNA with sequence designed to match the experimental construct, and 2) TRBP-dsRBD2, also designed to encompass the same residues as those present in the experimental construct, complexed with the GC 20-mer dsRNA. For simplicity, system 1 will be referred to as apo-RNA and system 2 will be referred to as holo-RNA. The apo-RNA system was constructed in UCSF Chimera (21) by building a self-complementary duplex with A-form geometry. The initial topology for the holo-RNA system was taken from the crystal structure of TRBP-dsRBD2 bound to coaxially stacked RNA duplexes (PDB: 3ADL) (15). To generate the simulated complex, GC20 was superimposed onto the crystallographic RNA, which was then deleted from the system, leaving a complex between TRBP-dsRBD2 and the intact 20-mer duplex. The disordered tails of the experimental TRBP-dsRBD2 construct extended beyond the deposited crystallographic model. Therefore, the missing residues were built in an extended

TABLE 1 Thermodynamic Parameters of TRBP-dsRBD2 Binding to GC20

T (K)	[TRBP-dsRBD2] (μM)	ΔH ($kcal \cdot mol^{-1}$)	ΔG ($kcal \cdot mol^{-1}$)	K_D (μM)	n (sites)
283	74	−6.90 ± 0.20	−8.00 ± 0.05	0.69 ± 0.07	4.86 ± 0.09
288	60	−6.10 ± 0.10	−8.38 ± 0.06	0.45 ± 0.05	4.79 ± 0.08
293	60	−5.62 ± 0.09	−8.70 ± 0.05	0.33 ± 0.03	4.86 ± 0.06
298	62	−5.87 + 0.09	−8.81 ± 0.05	0.35 ± 0.03	4.93 ± 0.06

conformation using UCSF Chimera (21). The tleap module of AmberTools 12.0 was used to construct the solvation box for each system (22). For the apo-RNA system, a cubic solvation box with dimensions of 92.1 Å was employed such that no RNA atom was within 10 Å of a box face, resulting in a total of 21,339 SPC/E water molecules being modeled. This system also required the placement of 58 Na^+ ions and 20 Cl^- ions to maintain charge neutrality. Similarly, for the holo-RNA system, a cubic solvation box with dimensions of 97.8 Å was employed, resulting in a total of 25,573 SPC/E water molecules being modeled. Charge neutrality was maintained for this system through the placement of 39 Na^+ ions and 6 Cl^- ions.

MD simulations

MD simulations were performed on the apo- and holo-RNA systems using the AMBER 12.0 Molecular Dynamics Package. Initial topology files for the systems were rendered using the Amber 99SB force field for the protein (23,24), and the Amber99 force field for the RNA, modified to include the Barcelona (BSC0) corrections for the α/γ RNA backbone torsions (25), and the χOL3 correction for the glycosidic torsion (26). It is important to note that the Amber99 force field generates A′-form RNA, which is characterized by a larger major groove compared with A-form RNA. Although this precludes a quantitative comparison of our simulation results with the original crystal structures, the qualitative trends revealed by the simulations are expected to have merit. Before the production runs, both systems were energy minimized and equilibrated as previously described (27,28). After equilibration, production simulations were performed in the NPT ensemble for 250 ns per system, with a 2 fs time step and a frame save-down rate of 1/ps. Trajectory analysis was completed using the cpptraj module of AmberTools 14.0, Curves+ (29), and in-house-written MATLAB scripts. The systems were visualized using UCSF Chimera and Visual Molecular Dynamics (30).

RESULTS AND DISCUSSION

CD analysis of TRBP-dsRBD2 binding stoichiometry on GC20 dsRNA

Previously published experimental results for the binding of a fully complementary 22-mer of dsRNA (ds22) by TRBP-dsRBD1 and TRBP-ΔC (both dsRBD1 and dsRBD2 together) are summarized in Fig. 1 *C* (7). Binding of ds22 by these two TRBP constructs is characterized by saturating stoichiometries of 5.0 ± 1.0 TRBP-dsRBD1 and 2.2 ± 0.3 TRBP-ΔC (equivalent to 4.4 dsRBDs) per ds22 duplex. Motivated by the crystal structures of TRBP and Xlrbpa-2 bound to dsRNA, in this study we used a GC 20-mer of RNA constructed to mimic the extended helix observed in the crystallographic models. We monitored the titrations of TRBP-dsRBD2 into GC20 using CD spectroscopy and observed a change in the ellipticity characteristic of dsRBD-dsRNA interactions (Fig. 1 *D*). The stoichiometry of this binding event was found to be 4.0 ± 1.0 TRBP-dsRBD2 per GC20, which, within the limits of our experimental uncertainties, is in excellent agreement with the previous results summarized here. Taken together, these results suggest that a consistent number of dsRBDs should be able to saturate an ideally Watson-Crick basepaired dsRNA of a given length (here approximately two turns of the A-form helix, 20–22 bp), irrespective of the identity of the dsRBD or the sequence of the dsRNA.

ITC analysis of TRBP-dsRBD2 binding to GC20 dsRNA

Crystallography has provided excellent insights into binding-mediated conformational changes that occur during sequence-specific protein-nucleic acid complex formation. For instance, the TATA-box binding protein (TBP) binds in a sequence-specific manner to B-form DNA, causing the otherwise linear B-form DNA to bend by a substantial 74° at the binding site (31). In an even more extreme case, the *Escherichia coli* catabolite gene activator protein (CAP) distorts the helical geometry by 90°, in essence forming a DNA hairpin (32). Such bends are not unique to protein-DNA complexes, as demonstrated by the DEAD-box protein Vasa, which induces an ~45° bend in A-form dsRNA upon binding, forcing a wedge conformation that drives a subsequent RNA unwinding event (33). In a highly influential 1994 study, Spolar and Record (34) established a framework for estimating the extent to which conformational changes in proteins are coupled to protein-nucleic acid binding events. Their work was based on the experimental measurement of binding heat capacity changes (ΔC_p). Temperature-dependent ITC is an exceptionally powerful experimental technique that provides direct access to ΔC_p through the measured temperature dependence of the observed binding enthalpy. As reviewed above, it is important to know whether dsRNA binding by TRBP bends the duplex or preserves a straight helical geometry, as this will have downstream implications involving the cleavage of the pre-miRNA by Dicer. Therefore, we employed the technique of temperature-dependent ITC to characterize the thermodynamics of TRBP-dsRBD2 binding to GC20 and to test the hypothesis that dsRBD binding induces a conformational change (e.g., a bend) in the GC20 RNA duplex, as suggested by the CD results presented above.

Estimation of ΔC_p from a linear fit of ΔH as a function of absolute temperature assumes that binding and its associated conformational changes are the only processes that contribute significantly to the measured injection heats over the temperature range of the study. Importantly, this means that it is assumed that neither the protein nor the RNA undergo thermal denaturation over the temperature range of the experiment. Therefore, a logical starting point for this study involved the determination of the thermal denaturation midpoint temperature for TRBP-dsRBD2 and for GC20 by DSC (Fig. S1; see Table S1 for best-fit parameters). Guided by these values and the temperature at which the onset of TRBP-dsRBD2 denaturation became apparent in the DSC thermogram, we chose an upper temperature limit of 25°C for the ITC temperature series. Fig. 2 *A* presents ITC measurements obtained from the titration of TRBP-dsRBD2 into GC20 RNA at temperatures ranging from 10°C to 25°C in 5°C increments. These

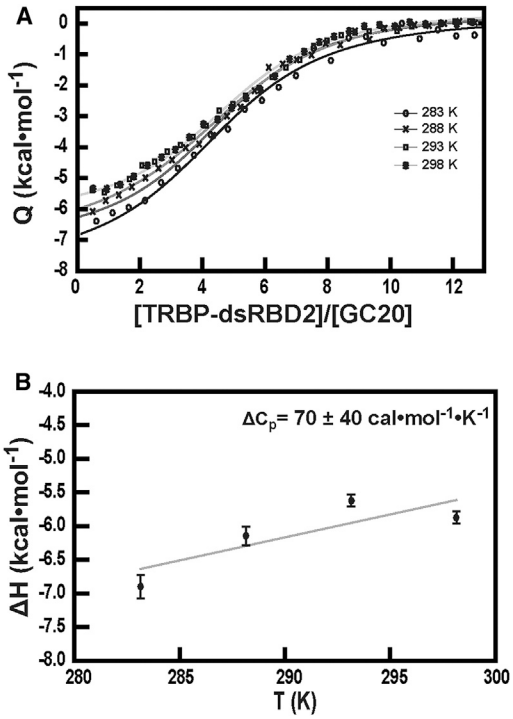

FIGURE 2 ITC temperature series. (*A*) Representative curves for titration of TRBP-dsRBD2 into GC20 dsRNA at 283 K (*open circles*), 288 K (*Xs*), 293 K (*open squares*), and 298 K (*stars*). (*B*) Change in enthalpy as a function of temperature. The plot shows the average enthalpy over three experiments at a given temperature, with error bars shown as one standard deviation. The specific heat of binding (ΔC_p) was calculated using the linear regression function in MATLAB, as described in Materials and Methods, and the resulting best-fit line is displayed in gray.

titrations reveal a small increase in ΔH_{obs} over the measured temperature range, which produces a small and positive ΔC_p (numerical values of best-fit parameters are provided in Table 1). The formation of this complex buries ~740 Å^2 of nonpolar surface area, which is likely to be an underestimate because the surface of a 20 bp duplex saturated with four or five dsRBDs is likely to be quite crowded, leading to the burial of additional surfaces. Given these considerations, the magnitude of the observed heat capacity is quite small, especially when compared with those observed for sequence-specific protein-nucleic acid complexes. For instance, using Spolar and Record's (34) formula, the TRBP-dsRBD2 interaction with GC20 should yield a heat capacity change associated with the hydrophobic effect of -140 cal$\cdot$K$^{-1}\cdot$mol^{-1}, which is strikingly different from our observed $\Delta C_p = 70 \pm 40$ cal$\cdot$K$^{-1}\cdot$mol^{-1} in both magnitude and sign. By comparison, the sequence-specific DNA-binding protein TrpR, which undergoes a structural rearrangement upon binding, forms a protein-DNA complex that buries 945 Å^2 of nonpolar surface area and yields a corresponding observed heat capacity change of $\Delta C_p = -220$ cal$\cdot$K$^{-1}\cdot$mol^{-1} (34). The positive sign of our observed ΔC_p is likely due to end effects attributable to our short dsRNA, which have been shown to generate similar small but positive ΔC_p values in studies of linkage between RNA duplex formation and monovalent salt binding (35). Given the small magnitude of the observed ΔC_p for TRBP-dsRBD2 binding to GC20 dsRNA, it seems unlikely that the formation of this complex is accompanied by any large-scale conformational changes.

MD simulations of GC20 and its complex with TRBP-dsRBD2

MD simulations can provide critical insights regarding the formation of protein-RNA complexes by characterizing the conformational dynamics available in these complexes. To attach a molecular picture to the thermodynamic data presented above, we generated 250 ns MD trajectories for both apo-GC20 and its complex with TRBP-dsRBD2. We generated the initial structure for the protein-dsRNA complex by constructing an ideal A-form 20-mer RNA (identical in sequence to the experimental GC20 duplex) and superimposing this duplex onto the crystallographic dsRNA in the holo-state structure of TRBP-dsRBD2 (see Materials and Methods). Both simulations were stable over the 250 ns of production dynamics (Fig. S2) and strong protein-RNA contacts were maintained (Figs. S3 and S4). Here, the conformational dynamics of the apo-GC20 and holo-RNA in complex elucidated by our MD simulations enable us to provide a straightforward test of the hypothesis that dsRBD binding induces a bend (or similar deformation) in the dsRNA.

It is well established that helix 2 of the dsRBD fold forms indispensable interactions with the major groove of the dsRNA (for TRBP-dsRBD2 the key residues are K210, K211, K214, and R215) (2,4,36). Notably, we have demonstrated that alanine mutations in this region of TRBP-dsRBD2 abrogate binding to dsRNA (7). In addition to the major-groove interactions mediated by helix 2, two sets of contacts between dsRBDs and the minor groove of the dsRNA are also important for RNA binding. There are three residues in helix 1 (H159, Q165, and Q166) contacting the 2′-hydroxyl group along minor groove 1, as well as three residues of loop 2 (H188, R189, and R190) contacting the sugar rings of minor groove 2 (15). To confirm that the MD simulations of the holo-RNA system demonstrate these significant contacts, we measured the distances between every residue in TRBP-dsRBD2 and the dsRNA for which there was a potential hydrogen-bonding interaction, using a 3.5 Å distance cutoff. The results are summarized in Fig. 3, where the relative occupancy of the hydrogen-bonded state is indicated by the color of the residue (the total hydrogen-bond occupancy is provided as Fig. S5). Violet residues exhibit a minimum of 70% occupancy, whereas lilac residues exhibit a minimum of 30% occupancy and pink residues exhibit a minimum of 10% occupancy. The binding interface within the major groove of the dsRNA is depicted in Fig. 3 *A*, where it can

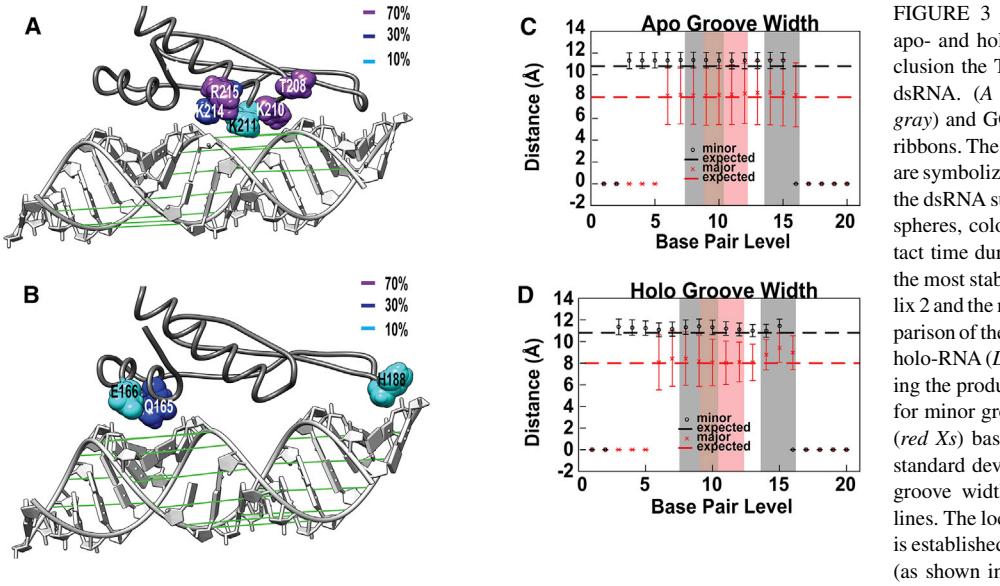

FIGURE 3 Determination of groove widths for apo- and holo-RNA trajectories supports the conclusion the TRBP-dsRBD2 binding does not bend dsRNA. (*A* and *B*) Both TRBP-dsRBD2 (*dark gray*) and GC20 RNA (*light gray*) are depicted as ribbons. The major (*A*) and minor (*B*) groove widths are symbolized by green lines. Residues that contact the dsRNA sugar-phosphate backbone are shown as spheres, color-coded to represent the percent contact time during the 250 ns MD simulation. All of the most stable contacts are between residues in helix 2 and the major groove of GC20. (*C* and *D*) Comparison of the average per-residue apo-RNA (*C*) and holo-RNA (*D*) groove-width distances sampled during the production MD trajectories. Average values for minor groove (*black circles*) and major groove (*red Xs*) basepair distances are shown along with standard deviations. The expected values for each groove width are represented as vertical dashed lines. The locations where protein-RNA interaction is established in the major groove and minor groove (as shown in *A* and *B*) are denoted by shaded regions, with the major-groove contacts shaded in pink and the minor-groove contacts in gray.

be seen that five protein residues participate in significant hydrogen bonding, with the strongest of these interactions involving K214, K210, and T208. A similar representation is depicted in Fig. 3 *B* for both minor grooves of the dsRNA. In these regions of the interface, only three additional hydrogen bonds display significant occupancy, which in all cases is less than that observed for the residues from helix 2 highlighted above. The highest occupancy within this region occurs at Q165 (~30%). These results are in good agreement with the literature and showcase the importance of specific contacts within the major groove for establishing a strong dsRBD-dsRNA interaction. Having demonstrated that these MD simulations recapitulate significant elements that are generally accepted as being diagnostic of dsRBD-dsRNA interactions, we went on to compare the apo- and holo-RNA trajectories in an attempt to elucidate any conformational changes that resulted from the dsRBD-dsRNA interaction.

As a simple means to assess RNA bending, we examined the average major- and minor-groove widths in the apo- and holo-RNA, as well as the magnitudes of their fluctuations, on a per-residue basis. As stated in the Materials and Methods, it is important to note that the Amber99 force field generates A′-form RNA, which is characterized by a larger major groove compared with A-form RNA. Fig. 3, *C* and *D*, show calculations of the apo- and holo-RNA groove widths, respectively, as measured by Curves+ (see Table 2 for a summary of output). The average major- and minor-groove widths are indicated by the red and black points, respectively, and the error bars depict their standard deviations. The expected values for the major- and minor-groove widths (*red and black dashed lines*, respectively) for a linear A′-form helix geometry are also included for reference. The major- and minor-groove widths are depicted visually by the green lines in Fig. 3, *A* (major) and *B* (minor). Fig. 3 *C* demonstrates that both the major- and minor-groove widths of the apo-RNA trajectory fall within the expected range for a linear A′-form helix. Additionally, it is noteworthy that the standard deviations determined for the major-groove widths are significantly larger than those obtained for the minor groove. Overall, these groove-width results, coupled with the root mean-square deviation values of the apo-RNA trajectory (Fig. S2), suggest that the helical geometry of the apo-RNA was well preserved throughout the simulation (i.e., no noticeable bending occurred). Strikingly, Fig. 3 *D* shows that the major- and minor-groove widths of the holo-RNA trajectory also fall within the expected range for a linear A′-form helix. Although there is a marginal increase in the average major-groove width of the holo-RNA trajectory, which coincides with the positions of those residues interacting with helix 2 (Fig. 3 *C*), the overall trend remains the same as that of the apo-RNA trajectory. What does change substantially between the apo- and holo-RNA simulations is the amplitude of the fluctuations in major-groove width measured for several base-pairs that make strong contact with TRBP, as implied in the smaller uncertainties represented in Fig. 3 *D*. Plots of

TABLE 2 Average Helical Parameter Results from MD Trajectories of Apo- and Holo-RNA

	A′-form RNA	Apo-RNA	Holo-RNA
Helical rise	3.0°	2.6° ± 0.4°	2.7° ± 0.4°
Helical twist	30°	31° ± 5°	29° ± 6°
X-displacement (Å)	−5.3	−4.0 ± 0.8	−4.0 ± 0.8
Major GW (Å)	8.0	6 ± 3	6 ± 2
Minor GW (Å)	10.8	10.0 ± 0.6	10.0 ± 6
Inclination	10.3°	15° ± 6°	14° ± 7°
Axial bend	–	1.7° ± 0.9°	2.6° ± 0.4°

the groove widths at each basepair position are presented as a function of time in Figs. S6 and S7. Specifically, whereas basepairs 12–15 sample conformational states spanning the same range of major-groove distances in both simulations, the holo-RNA simulation features discrete jumps between a narrow-groove and a wide-groove state, with a substantially reduced fluctuation magnitude within a given state (Fig. S6). It is interesting to speculate that the altered fluctuations observed here may contribute to both the small and positive observed ΔCp and the change in CD signal that is used to evaluate binding stoichiometry in Fig. 1. Finally, Table 2 shows that there is no appreciable difference in the axial bend of the apo- and holo-RNA trajectories. Taken together, our MD results clearly indicate a lack of appreciable distortion of the helical geometry of the dsRNA as a result of interaction with TRBP-dsRBD2.

CONCLUSIONS

Although Dicer is able to process pre-miRNA in the absence of TRBP, the formation of a Dicer-TRBP complex has been shown to influence processing-site selection (12), which was recently shown to impact guide-strand selection (13). Therefore, enhancing our understanding of the mechanism whereby TRBP binds to dsRNA has potentially far-reaching implications for understanding and manipulating gene silencing by miRNA. Here, both experimental and computational techniques were employed to examine the hypothesis that TRBP-dsRBD2 binding by a 20-mer dsRNA is coupled with RNA bending. This investigation focused on complex formation between TRBP-dsRBD2 and a 20-mer GC-duplex intended to mimic the RNA oligonucleotides used in historically significant cocrystal structures of dsRBD-dsRNA complexes. In the complex of TRBP-dsRBD2 with 10-mer alternating GC-dsRNA, the crystallographic model revealed widening of the major groove of the dsRNA (in the region of a nonbiological double-strand break in the RNA), which was speculated to be required to accommodate helix 2 from the dsRBD. Analysis of the binding thermodynamics for TRBP-dsRBD2 interactions with GC20, recorded through temperature-dependent ITC experiments, yielded a small and positive ΔC_p associated with the binding event. In comparison with theoretical values calculated using well-established techniques, this change in heat capacity suggests that large conformational changes are unlikely to result from the dsRBD-dsRNA interactions in this system. This conclusion is corroborated by MD simulations suggesting that there are no appreciable differences in the major- and minor-groove widths or axial bends induced in the dsRNA through interaction with TRBP-dsRBD2. TRBP operates in conjunction with the catalytic enzyme Dicer to properly cleave the apical loop of precursor miRNA (~33 bp in length) into a dsRNA duplex termed miRNA/miRNA* (~22 bp in length). We have previously shown that TRBP's observed dsRNA equilibrium binding constant scales monotonically with the duplex length in this range. Significantly, we have also shown that TRBP does not readily bind to regions with helical deformations (e.g., bulges and mismatches), which are ubiquitous in the precursor forms of miRNA. In combination with the findings in this study, our work suggests that in vivo, TRBP's role in miRNA maturation is to bind pre-miRNA in the helical regions, avoiding segments of imperfect double-helical structure and thereby establishing the cut-site position for Dicer cleavage.

SUPPORTING MATERIAL

Supporting Materials and Methods, seven figures, and one table, are available at http://www.biophysj.org/biophysj/supplemental/S0006-3495(16)30289-2.

AUTHOR CONTRIBUTIONS

R.A. designed research, performed CD and ITC experiments, analyzed data, and wrote the manuscript. D.E. performed DSC and ITC experiments, analyzed data, and wrote the manuscript. K.A.P. analyzed data and wrote the manuscript. S.A.S. designed research, performed the MD simulations, analyzed data, and wrote the manuscript.

ACKNOWLEDGMENTS

We thank Dr. Philip Bevilacqua for use of the Jasco CD spectrometer, and Dr. Debashish Sahu for helpful discussions about MATLAB.

This work was supported by U.S. National Institutes of Health grant R01GM098451 to S.A.S.

REFERENCES

1. Gatignol, A., A. Kumar, …, K. T. Jeang. 1989. Identification of cellular proteins that bind to the human immunodeficiency virus type 1 transactivation-responsive TAR element RNA. *Proc. Natl. Acad. Sci. USA*. 86:7828–7832.
2. Tian, B., P. C. Bevilacqua, …, M. B. Mathews. 2004. The double-stranded-RNA-binding motif: interference and much more. *Nat. Rev. Mol. Cell Biol.* 5:1013–1023.
3. Pratt, A. J., and I. J. MacRae. 2009. The RNA-induced silencing complex: a versatile gene-silencing machine. *J. Biol. Chem.* 284:17897–17901.
4. Masliah, G., P. Barraud, and F. H. Allain. 2013. RNA recognition by double-stranded RNA binding domains: a matter of shape and sequence. *Cell. Mol. Life Sci.* 70:1875–1895.
5. Wostenberg, C., K. A. Quarles, and S. A. Showalter. 2010. Dynamic origins of differential RNA binding function in two dsRBDs from the miRNA "microprocessor" complex. *Biochemistry.* 49:10728–10736.
6. Wostenberg, C., J. W. Lary, …, S. A. Showalter. 2012. The role of human Dicer-dsRBD in processing small regulatory RNAs. *PLoS One.* 7:e51829.
7. Acevedo, R., N. Orench-Rivera, …, S. A. Showalter. 2015. Helical defects in microRNA influence protein binding by TAR RNA binding protein. *PLoS One.* 10:e0116749.
8. Sohn, S. Y., W. J. Bae, …, Y. Cho. 2007. Crystal structure of human DGCR8 core. *Nat. Struct. Mol. Biol.* 14:847–853.

9. Yamashita, S., T. Nagata, …, S. Yokoyama. 2011. Structures of the first and second double-stranded RNA-binding domains of human TAR RNA-binding protein. *Protein Sci.* 20:118–130.
10. Lee, H. Y., K. Zhou, …, J. A. Doudna. 2013. Differential roles of human Dicer-binding proteins TRBP and PACT in small RNA processing. *Nucleic Acids Res.* 41:6568–6576.
11. Roth, B. M., D. Ishimaru, and M. Hennig. 2013. The core microprocessor component DiGeorge syndrome critical region 8 (DGCR8) is a nonspecific RNA-binding protein. *J. Biol. Chem.* 288:26785–26799.
12. Lee, H. Y., and J. A. Doudna. 2012. TRBP alters human precursor microRNA processing in vitro. *RNA.* 18:2012–2019.
13. Wilson, R. C., A. Tambe, …, J. A. Doudna. 2015. Dicer-TRBP complex formation ensures accurate mammalian microRNA biogenesis. *Mol. Cell.* 57:397–407.
14. Ryter, J. M., and S. C. Schultz. 1998. Molecular basis of double-stranded RNA-protein interactions: structure of a dsRNA-binding domain complexed with dsRNA. *EMBO J.* 17:7505–7513.
15. Yang, S. W., H. Y. Chen, …, Y. A. Yuan. 2010. Structure of Arabidopsis HYPONASTIC LEAVES1 and its molecular implications for miRNA processing. *Structure.* 18:594–605.
16. Gan, J., J. E. Tropea, …, X. Ji. 2006. Structural insight into the mechanism of double-stranded RNA processing by ribonuclease III. *Cell.* 124:355–366.
17. Stefl, R., F. C. Oberstrass, …, F. H. Allain. 2010. The solution structure of the ADAR2 dsRBM-RNA complex reveals a sequence-specific readout of the minor groove. *Cell.* 143:225–237.
18. Greenfield, N. J. 2006. Using circular dichroism spectra to estimate protein secondary structure. *Nat. Protoc.* 1:2876–2890.
19. Ucci, J. W., Y. Kobayashi, …, J. L. Cole. 2007. Mechanism of interaction of the double-stranded RNA (dsRNA) binding domain of protein kinase R with short dsRNA sequences. *Biochemistry.* 46:55–65.
20. Sahu, D., M. Bastidas, …, S. A. Showalter. 2016. Assessing coupled protein folding and binding through temperature-dependent isothermal titration calorimetry. *Methods Enzymol.* 567:23–45.
21. Pettersen, E. F., T. D. Goddard, …, T. E. Ferrin. 2004. UCSF Chimera—a visualization system for exploratory research and analysis. *J. Comput. Chem.* 25:1605–1612.
22. Pearlman, D. A., D. A. Case, …, P. Kollman. 1995. AMBER, a package of computer programs for applying molecular mechanics, normal mode analysis, molecular dynamics and free energy calculations to simulate the structural and energetic properties of molecules. *Comput. Phys. Commun.* 91:1–41.
23. Hornak, V., A. Okur, …, C. Simmerling. 2006. HIV-1 protease flaps spontaneously open and reclose in molecular dynamics simulations. *Proc. Natl. Acad. Sci. USA.* 103:915–920.
24. Hornak, V., R. Abel, …, C. Simmerling. 2006. Comparison of multiple Amber force fields and development of improved protein backbone parameters. *Proteins.* 65:712–725.
25. Zgarbová, M., F. J. Luque, …, P. Jurečka. 2013. Toward improved description of DNA backbone: revisiting epsilon and zeta torsion force field parameters. *J. Chem. Theory Comput.* 9:2339–2354.
26. Zgarbová, M., M. Otyepka, …, P. Jurečka. 2011. Refinement of the Cornell et al. nucleic acids force field based on reference quantum chemical calculations of glycosidic torsion profiles. *J. Chem. Theory Comput.* 7:2886–2902.
27. Showalter, S. A., and R. Brüschweiler. 2007. Validation of molecular dynamics simulations of biomolecules using NMR spin relaxation as benchmarks: application to the AMBER99SB force field. *J. Chem. Theory Comput.* 3:961–975.
28. Wostenberg, C., W. G. Noid, and S. A. Showalter. 2010. MD simulations of the dsRBP DGCR8 reveal correlated motions that may aid pri-miRNA binding. *Biophys. J.* 99:248–256.
29. Lavery, R., M. Moakher, …, K. Zakrzewska. 2009. Conformational analysis of nucleic acids revisited: Curves+. *Nucleic Acids Res.* 37:5917–5929.
30. Humphrey, W., A. Dalke, and K. Schulten. 1996. VMD: visual molecular dynamics. *J. Mol. Graph.* 14:33–38, 27–38.
31. Kim, Y., J. H. Geiger, …, P. B. Sigler. 1993. Crystal structure of a yeast TBP/TATA-box complex. *Nature.* 365:512–520.
32. Parkinson, G., C. Wilson, …, H. M. Berman. 1996. Structure of the CAP-DNA complex at 2.5 angstroms resolution: a complete picture of the protein-DNA interface. *J. Mol. Biol.* 260:395–408.
33. Sengoku, T., O. Nureki, …, S. Yokoyama. 2006. Structural basis for RNA unwinding by the DEAD-box protein Drosophila Vasa. *Cell.* 125:287–300.
34. Spolar, R. S., and M. T. Record, Jr. 1994. Coupling of local folding to site-specific binding of proteins to DNA. *Science.* 263:777–784.
35. Takach, J. C., P. J. Mikulecky, and A. L. Feig. 2004. Salt-dependent heat capacity changes for RNA duplex formation. *J. Am. Chem. Soc.* 126:6530–6531.
36. Gleghorn, M. L., and L. E. Maquat. 2014. 'Black sheep' that don't leave the double-stranded RNA-binding domain fold. *Trends Biochem. Sci.* 39:328–340.